Molecular Imaging
Volume 16 : 1-11

DOI: 10.1177/1536012117724558
journals.sagepub.com/home/mix
SAGE

Longitudinal Evaluation of Myocardial Fatty Acid and Glucose Metabolism in Fasted and Nonfasted Spontaneously Hypertensive Rats Using MicroPET/CT

Jennifer S. Huber, PhD[1], Andrew M. Hernandez, PhD[2], Mustafa Janabi, PhD[1], James P. O'Neil, PhD[1], Kathleen M. Brennan, DVM[1], Stephanie T. Murphy, BS[3], Youngho Seo, PhD[1,3,4,5], and Grant T. Gullberg, PhD[1,3,5]

Abstract

Using longitudinal micro positron emission tomography (microPET)/computed tomography (CT) studies, we quantified changes in myocardial metabolism and perfusion in spontaneously hypertensive rats (SHRs), a model of left ventricular hypertrophy (LVH). Fatty acid and glucose metabolism were quantified in the hearts of SHRs and Wistar-Kyoto (WKY) normotensive rats using long-chain fatty acid analog ^{18}F-fluoro-6-thia heptadecanoic acid (^{18}F-FTHA) and glucose analog ^{18}F-fluorodeoxyglucose (^{18}F-FDG) under normal or fasting conditions. We also used ^{18}F-fluorodihydrorotenol (^{18}F-FDHROL) to investigate perfusion in their hearts without fasting. Rats were imaged at 4 or 5 times over their life cycle. Compartment modeling was used to estimate the rate constants for the radiotracers. Blood samples were obtained and analyzed for glucose and free fatty acid concentrations. SHRs demonstrated no significant difference in ^{18}F-FDHROL wash-in rate constant ($P = .1$) and distribution volume ($P = .1$), significantly higher ^{18}F-FDG myocardial influx rate constant ($P = 4\times10^{-8}$), and significantly lower ^{18}F-FTHA myocardial influx rate constant ($P = .007$) than WKYs during the 2009-2010 study without fasting. SHRs demonstrated a significantly higher ^{18}F-FDHROL wash-in rate constant ($P = 5\times10^{-6}$) and distribution volume ($P = 3\times10^{-8}$), significantly higher ^{18}F-FDG myocardial influx rate constant ($P = 3\times10^{-8}$), and a higher trend of ^{18}F-FTHA myocardial influx rate constant (not significant, $P = .1$) than WKYs during the 2011–2012 study with fasting. Changes in glucose plasma concentrations were generally negatively correlated with corresponding radiotracer influx rate constant changes. The study indicates a switch from preferred fatty acid metabolism to increased glucose metabolism with hypertrophy. Increased perfusion during the 2011-2012 study may be indicative of increased aerobic metabolism in the SHR model of LVH.

Keywords

animal models of disease, quantitation in molecular imaging, cardiovascular, animal pet, cardiac imaging, molecular modeling

[1] Molecular Biophysics and Integrated Bioimaging Division, Lawrence Berkeley National Laboratory, Berkeley, CA, USA
[2] Department of Radiology, University of California Davis, Sacramento, CA, USA
[3] Department of Radiology and Biomedical Imaging, University of California, San Francisco, CA, USA
[4] Department of Radiation Oncology, University of California, San Francisco, CA, USA
[5] UC Berkeley—UCSF Graduate Program in Bioengineering, Berkeley and San Francisco, CA, USA

Submitted: 17/01/2017. Revised: 25/05/2017. Accepted: 01/07/2017.

Corresponding Author:
Grant T. Gullberg, UCSF Physics Research Laboratory, University of California San Francisco, 185 Berry St, Ste 350, San Francisco, CA 94143, USA.
Email: gtgullberg@lbl.gov

Introduction

Left ventricular hypertrophy (LVH) is the enlargement, thickening, and stiffening of the muscle (myocardium) that makes up the wall of the main pumping chamber of the heart. Hypertrophy can develop in response to hypertension, characterized by high blood pressure that requires the LV to work harder. Ultimately, it can lead to heart failure (HF), when the heart no longer provides enough blood to meet the metabolic needs of the body.

Under healthy conditions, fatty acids (FAs) are the preferred metabolic fuel, accounting for 60% to 70% of energy production.[1,2] Fatty acids provide more than twice as much energy per mass than glucose. As hypertrophy develops, the heart exhibits impaired substrate metabolism, contractile dysfunction, and LV remodeling.[3] In this diseased state, it is believed that the heart switches to rely on glucose as the major fuel.

Molecular imaging using micro positron emission tomography (microPET) with 14(R,S)-^{18}F-fluoro-6-thia-heptadecanoic acid (^{18}F-FTHA) and 2-deoxy-2-^{18}F-fluoro-D-glucose (^{18}F-FDG) is used to estimate changes in FA and glucose metabolism, respectively, in response to cardiac stress due to cardiac hypertrophy and HF.[4,5] First synthesized by Degrado and Coenen[6] in 1991, ^{18}F-FTHA is transported into the myocardium, undergoes initial steps of β-oxidation, and subsequently is trapped in the cell.[6,7] Only a small fraction of ^{18}F-FTHA is incorporated into triglycerides. The rate of ^{18}F-FTHA retention by the myocardium is believed to reflect β-oxidation of the long-chain FA.[6] In addition, increased oxygen demands generated by the hypertrophied LV increase myocardial oxygen consumption in the failing heart.[8–10]

In order to quantify these changes in myocardial metabolism during the progression of hypertrophy, we performed 2 longitudinal microPET/computed tomography (CT) studies using spontaneously hypertensive rats (SHRs) and Wistar-Kyoto (WKY) control rats. The SHR is a model of LVH and HF.[11,12] It has a genetic deletion variant in the CD36 FA transporter,[13] resulting in defective FA metabolism, insulin resistance, hypertension, and ultimately progression of LVH with age.

The purpose of these microPET/CT rat studies was to noninvasively quantify the longitudinal alterations in myocardial metabolism and perfusion in the SHR as a model of LVH and to compare these alterations with WKY controls. In addition, the studies investigated the effect of fasting and feeding on these processes. The molecular imaging techniques that we have developed to monitor substrate metabolism shifts during the progression of HF could be translated directly to humans, in order to help improve diagnosis, risk stratification, and therapy management for patients with HF.

Materials and Methods

Our first longitudinal imaging study in 2009 to 2010 tracked changes in glucose metabolism, FA metabolism, and perfusion as a function of hypertrophy and age in separate rat cohorts over their life cycle. Our second imaging study[14] in 2011 to 2012 tracked changes in all of these physiological processes in a single rat cohort over their life cycle. In the first study, the rats were fed freely, and in the second study, the rats were fasted overnight prior to imaging, thus we have also investigated the effects of fasting.

We used the long-chain FA analog ^{18}F-FTHA and glucose analog ^{18}F-FDG PET radiotracers to image the rats under fed or fasted conditions. We also evaluated ^{18}F-fluorodihydrorotenol (^{18}F-FDHROL), an analog of the mitochondrial complex I substrate rotenone, as an indicator of perfusion in the heart.

Synthesis of Radiotracers

^{18}F-FDG was synthesized at the University of California San Francisco (UCSF) Radiopharmaceutical Facility using the TRACERlab MX synthesis module (GE Healthcare, Chicago, Illinois). Both ^{18}F-FTHA and ^{18}F-FDHROL were synthesized at UCSF[15] using the TRACERlab FxFN synthesis module (GE Healthcare, Chicago, Illinois).

Animal Study Design

All imaging studies were performed in accordance with Institutional Animal Care and Use Committee–approved protocols from both UCSF and Lawrence Berkeley National Laboratory. The SHRs and WKY control rats were imaged at 4 to 5 time points over their life cycle for each protocol.

The 2009 to 2010 Study

For the 2009 to 2010 study, 16 male SHRs and 16 male WKY normotensive rats were purchased from Charles River Laboratories (Wilmington, Massachusetts). Imaging of 3 separate cohorts began at approximately 6 to 9 months of age. Cohort 1 (8 SHR, 8 WKY) was imaged with ^{18}F-FDHROL at the age of 6, 12, 16, 18, and 21 months. Cohort 2 (4 SHR, 4 WKY) was imaged with ^{18}F-FDG at the age of 7, 12, 16, and 20 months. Cohort 3 (4 SHR, 4 WKY) was imaged with ^{18}F-FTHA at the age of 9, 12, 16, 19, and 21 months. All rats were freely fed standard Purina rat chow and water. The rats were not fasted before any of the imaging studies.

The 2011 to 2012 Study

For the 2011 to 2012 study, 8 male SHRs and 8 male WKY normotensive rats were purchased from Charles River Laboratories. A single rat cohort of 8 SHR and 8 WKY was imaged using all 3 radiotracers during each time point. Imaging began at approximately 8 months of age and the rats were imaged at separate time points corresponding to 8 to 9, 13 to 14, 19 to 20, and 22 to 23 months of age. During each time point, every rat was imaged using all 3 radiotracers (^{18}F-FDG, ^{18}F-FTHA, and ^{18}F-FDHROL) on separate days and separate anesthetic applications. All rats were normally freely fed standard Purina rat chow and water, eating mostly at night. Before ^{18}F-FDG and ^{18}F-FTHA imaging, food was taken away the evening before the studies, whereas the rats were not fasted for the ^{18}F-FDHROL studies.

Imaging Protocol

All in vivo imaging was performed using a microPET/CT scanner (Inveon; Siemens Molecular Solutions, Malvern, Pennsylvania). Each rat was anesthetized with ~2% isoflurane and oxygen. Electrocardiogram (ECG) electrodes were attached to the 2 front limbs and left hind limb to acquire triggering signals. Rats were positioned on the scanning bed with the heart centered in the field of view. Each radiotracer was administered via tail vein injection as a 0.5 to 1.5 mL bolus with activities of approximately 50 MBq.

Data acquisition began at the time of injection. Dynamic ECG-gated (BioVet System; m2m Imaging Corp, Cleveland, Ohio) list mode PET data were acquired over 60 minutes. After the PET acquisition, a CT scan was acquired with 120 projections of continuous rotation to cover 220° with an X-ray tube operated at 80 kVp, 0.5 mA, and 160 milliseconds exposure time.

Image Analysis

All PET data were reconstructed into 8 cardiac gates of 38 time frames (12 × 5 seconds, 6 × 10 seconds, 4 × 30 seconds, 6 × 60 seconds, and 10 × 300 seconds). The 2-D ordered subsets expectation maximization algorithm provided by the scanner manufacturer was used for the PET reconstruction. Reconstruction resulted in 128 × 128 × 159 matrices with a voxel size of 0.78 × 0.78 × 0.80 mm^3. The CT image was reconstructed using a cone beam Feldkamp reconstruction algorithm (COBRA) supplied by Exxim Computing Corporation (Pleasanton, California) with a matrix size of 512 × 512 × 662 and a voxel size of 0.19 × 0.19 × 0.19 mm^3. Photon attenuation correction was achieved using the co-registered CT-based attenuation map.

The ECG gating was used to subdivide data sets into 8 cardiac phases to minimize cardiac motion, spillover contamination, and partial volume effects. Diastolic bins of 2 to 3 cardiac phases were identified and new dynamic image sequences were formed by summing counts in each identified diastolic bin. By summing just the diastolic bins (Figure 1), we improved the boundary definition in the LV myocardium. We have found even though counts are sacrificed by creating a dynamic sequence during the diastolic phase of the cardiac cycle, this approach provided more accurate time–activity curves (TACs) and estimated kinetic parameters.

The new dynamic series of framed diastolic bins were then uploaded into the Inveon Research Workplace version 3.0 (Siemens Molecular Solutions, Malvern, Pennsylvania) software platform. Myocardial TACs (Figure 2) were generated by manually drawing a volume of interest (VOI) in the myocardium, with care taken to avoid the myocardial border. Both ^{18}F-FTHA and ^{18}F-FDHROL images displayed more liver uptake than ^{18}F-FDG images in both rat models (Figure 1). To minimize spillover of radioactivity from the liver to the heart, the entire apex and mid-cavity septal wall were not defined within the VOI for any ^{18}F-FTHA or ^{18}F-FDHROL images. Tissue VOIs were selected by placing voxels in 10 consecutive midventricle slices. Only slices containing myocardium in 360° were selected. The VOI consisted of approximately 50 voxels.

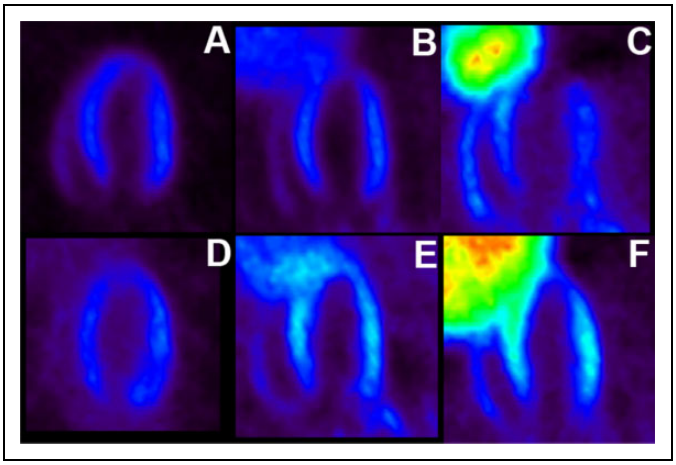

Figure 1. Example of reconstructed microPET images. A-C, The PET images corresponding to only ECG bins summed from 40 to 60 minutes. D-F, The PET images corresponding to only diastolic ECG bins summed from 40 to 60 minutes. A and D, ^{18}F-FDG image of SHR showing almost no liver uptake; (B and E), ^{18}F-FDHROL image of SHR showing substantial liver uptake; (C and F), ^{18}F-FTHA image of SHR again showing substantial liver uptake. ECG, electrocardiogram; FDG, fluorodeoxyglucose; FDHROL, fluorodihydrorotenol; FTHA, fluoro-6-thia-heptadecanoic acid; PET, positron emission tomography; SHR, spontaneously hypertensive rat.

Blood TACs were generated for each tracer using a small region of interest (10-20 mm^3) within the LV blood pool, with care taken to avoid the boundary between the myocardium and LV cavity. The diastolic PET images provided clear definition of myocardium and blood pool regions, (see examples in Figure 1).

Determination of ^{18}F-FDHROL Wash-In Rate Constant

The TACs for the manually drawn volumes of interest in the LV myocardium and the blood input were fit to a 1-tissue compartment model to obtain the wash-in rate constant K_1 from the LV blood pool into the extravascular and cellular spaces of the myocardium, as well as the wash-out rate constant k_2 from out of the myocardium into the LV blood pool (Figure 3). We estimated the rate constants by fitting the ^{18}F-FDHROL TACs to this single-tissue model, using a standard Inveon Research Workplace (IRW) algorithm for the 2009 to 2010 study and a closed-form algorithm[16] for the 2011 to 2012 study. The distribution volume V_d was also calculated as the ratio of K_1 to k_2.

Determination of ^{18}F-FDG and ^{18}F-FTHA Influx Rate Constant

The 2-tissue compartment model in Figure 3 was used as a model of the kinetics of ^{18}F-FDG and ^{18}F-FTHA. It was assumed that ^{18}F-FDG is primarily trapped in the myocardium and is not released as one would infer from the TAC in Figure 2;

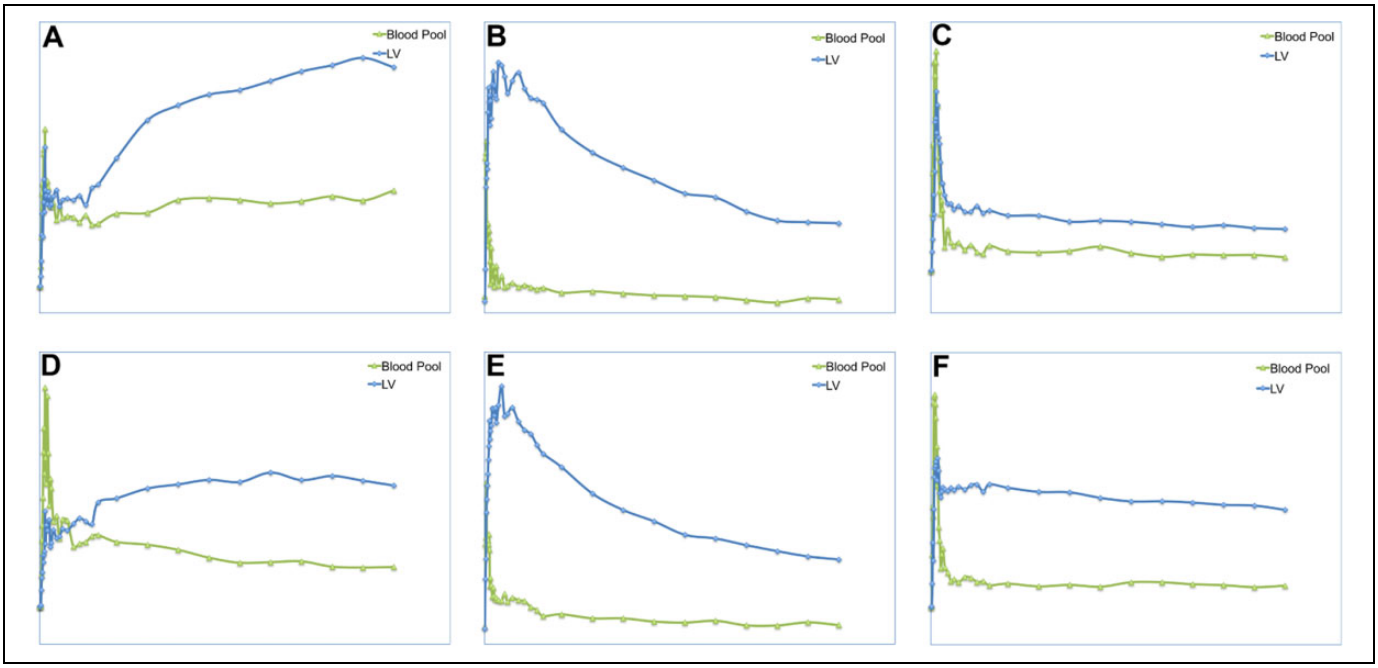

Figure 2. Example TACs for the entire 60-minute acquisition from 2009 to 2010 studies. A-C, Examples of TACs for blood and LV myocardium for SHR animals. D-F, Examples of TACs for blood and LV myocardium for WKY animals. A and D, ^{18}F-FDG TACs; (B and E) ^{18}F-FDHROL TACs; (C and F), ^{18}F-FTHA TACs. FDG indicates fluorodeoxyglucose; FDHROL, fluorodihydrorotenol; FTHA, fluoro-6-thia-heptadecanoic acid; LV, left ventricular; TACs, time–activity curves.

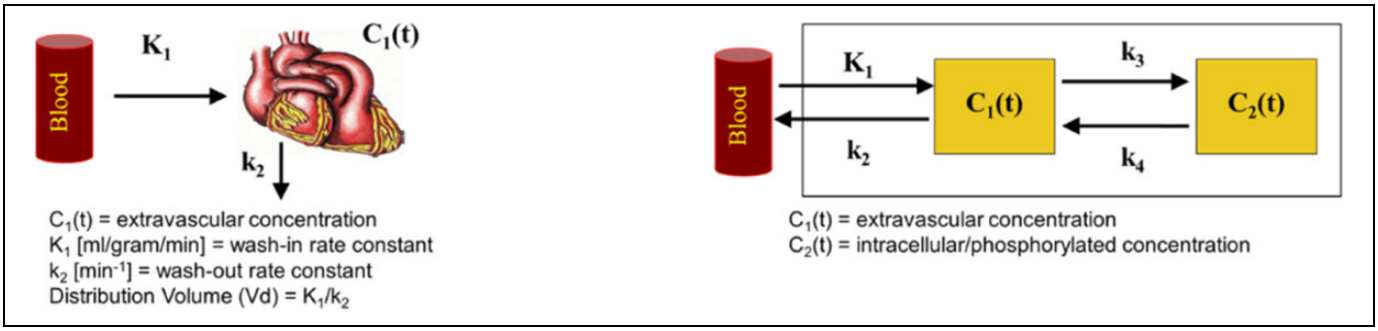

Figure 3. One-tissue compartment model (left) and 2-tissue compartment model (right) that model the perfusion and metabolic kinetics, respectively.

therefore, $k_4 = 0$. The myocardial influx rate constant K_i^{FDG} for ^{18}F-FDG was estimated using linear regression provided by the multiple-time Patlak graphical analysis.[4,17] On the other hand, ^{18}F-FTHA is slowly released from the myocardium as observed with the TAC in Figure 2; therefore, $k_4 \neq 0$ in Figure 3. However, in our analysis, we assumed that k_4 was small and used the Patlak graphical analysis to estimate the influx rate constant K_i^{FTHA} for ^{18}F-FTHA. For the Patlak graphical analysis, the last 10 time frames (10-60 minutes) were used to determine K_i^{FDG} and K_i^{FTHA}.

Glucose, Insulin, and FFA Analyses

Approximately 1 mL of blood was drawn from the tail vein of each rat immediately following either the ^{18}F-FDG or ^{18}F-FTHA imaging study. Each sample was spun in an Eppendorf 5415D microcentrifuge for 10 minutes at 10,000 rpm. The plasma was separated, immediately stored at −80°C, and then sent to Ani Lytics Inc. (Gaithersburg, MD, USA) Glucose, insulin, and FFA concentrations were measured using a Roche Hitachi 717 Chemistry Analyzer (Roche Diagnostics, Indianapolis, IN, USA).

Statistical Analysis

Two-way analysis of variance (ANOVA) was used to determine the main effect of contributions from each independent variable (i.e. rat model or time) and was also used to identify possible interaction effects between variables. In addition, Welch unpaired t test was used to compare the mean of the

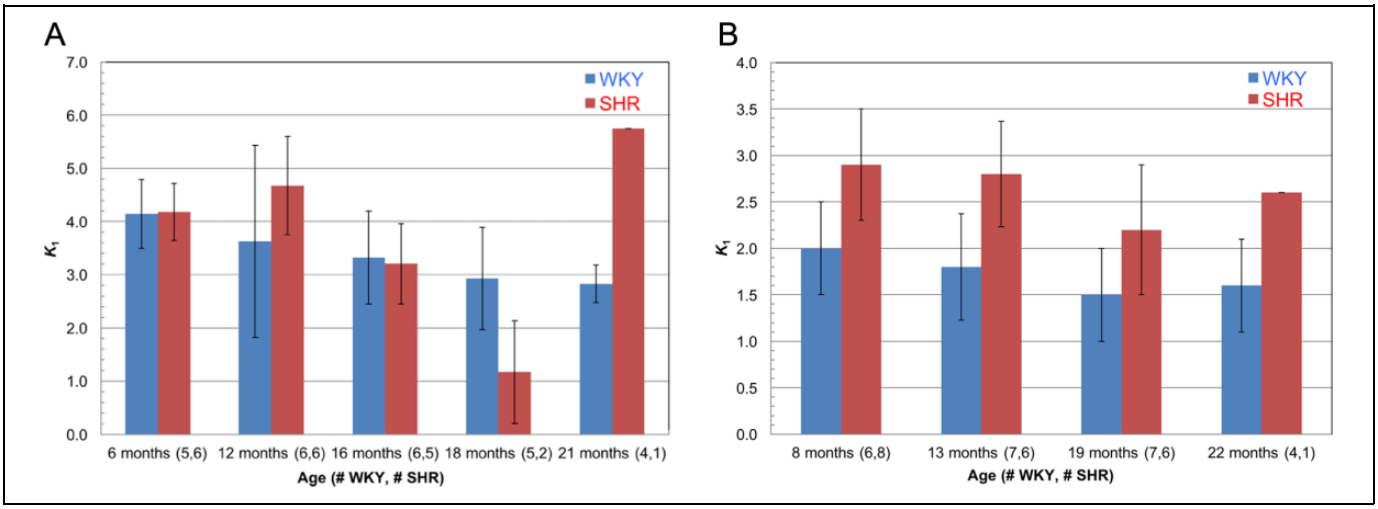

Figure 4. The ^{18}F-FDHROL wash-in rate constant (K_1) in myocardium as a function of age for the (A) 2009 to 2010 study and (B) 2011 to 2012 study. For both studies, the rats were not fasted. The 2009 to 2010 study was fit to a single-tissue compartment model using the standard nonlinear algorithm implemented in IRW provided by the scanner manufacturer, whereas the data from the 2011 to 2012 study were fit using an analytical closed-form method.[16] FDHROL indicates fluorodihydrorotenol; IRW, Inveon Research Workplace.

2 rat models with unequal variances at a given time point, as well as to compare the postmortem heart to body weight ratio. The use of Welch's unpaired *t*-test is indicated explicitly in this article. *P* values less than .05 were considered statistically significant for all tests.

Results

The number of rats imaged at each time point throughout the longitudinal study decreased because some of the rats died. The SHRs died because of cardiac failure due to cardiac hypertrophy. Some of the WKY rats were killed earlier than the 2 years because of fatty tumors. At times, there were acquisition problems where the animals moved and the data were not acceptable for analysis.

^{18}F-FDHROL Kinetics in Myocardial Tissue (Perfusion)

The TACs demonstrated that ^{18}F-FDHROL was rapidly taken up in the myocardium and rapidly extracted from the LV blood pool (Figure 2). The 1-tissue compartment model fit of the wash-in rate constants (K_1) is shown in Figure 4. A 2-way ANOVA indicated that the SHRs demonstrated a significantly higher ^{18}F-FDHROL wash-in rate constant ($P = 5 \times 10^{-6}$) and distribution volume ($P = 3 \times 10^{-8}$) than the WKY controls for the 2011 to 2012 study, whereas no significant difference for these factors was seen between rat models for the 2009 to 2010 study ($P = .1$; Table 1). The distribution volumes were 7.12 $\pm$ 2.07 (range: 5.40-9.54) and 9.03 $\pm$ 1.18 (range: 5.18-14.81) for WKY and SHR, respectively, in the 2009 to 2010 study, and 6.6 $\pm$ 1.6 (range: 6.0-7.6) and 10.3 $\pm$ 1.0 (range: 7.2-18.9) for WKY and SHR, respectively, in the 2011 to 2012 study. The distribution volume is expected to increase with hypertrophy due to an increase in collagen that creates an increase in interstitial space.

Table 1. Summary of Perfusion Results.

	2009 to 2010	2011 to 2012
FDHROL wash-in rate constant	Not significant	SHR > WKY
Distribution volume	Not significant	SHR > WKY

Abbreviations: FDHROL, fluorodihydrorotenol; SHR, spontaneously hypertensive rat; WKY, Wistar-Kyoto.

^{18}F-FDG Kinetics in Myocardial Tissue (Glucose)

The uptake of ^{18}FDG as a function of time in the WKY and SHR is shown in Figure 2. It is seen that the amount of glucose uptake (integral over time) was greater in the SHR than the WKY. It has been reported that isoflurane can produce a hyperglycemic effect.[19] This is probably why we consistently saw uptake in both the WKY and SHR, while in humans, it may be virtually nonvisible without glucose loading.

A 2-way ANOVA indicated that the SHRs demonstrated a significantly higher ^{18}F-FDG myocardial influx rate constant K_i^{FDG} than the WKY controls under both fed ($P = 4 \times 10^{-8}$) and fasted ($P = 3 \times 10^{-8}$) conditions (Figure 5). The ^{18}F-FDG influx rate constant K_i^{FDG} decreased with age for all rats when fasted ($P = .03$), but no significant trend was seen with age when fed ($P = .2$).

A 2-way ANOVA of blood data indicated that glucose concentrations were significantly lower for the SHRs than the WKY controls under fed ($P = 2 \times 10^{-6}$) and fasted ($P = 6 \times 10^{-12}$) conditions (Table 2). Moreover, when fasted, a significant age-dependent increase in glucose plasma concentration was apparent in the controls ($P < 2 \times 10^{-5}$) but not in the SHRs. In comparison, insulin concentrations were significantly higher for the SHRs than the WKY rats ($P = 3 \times 10^{-3}$) when fasted, whereas no significant difference was observed between models under fed conditions ($P = .4$). When fasted,

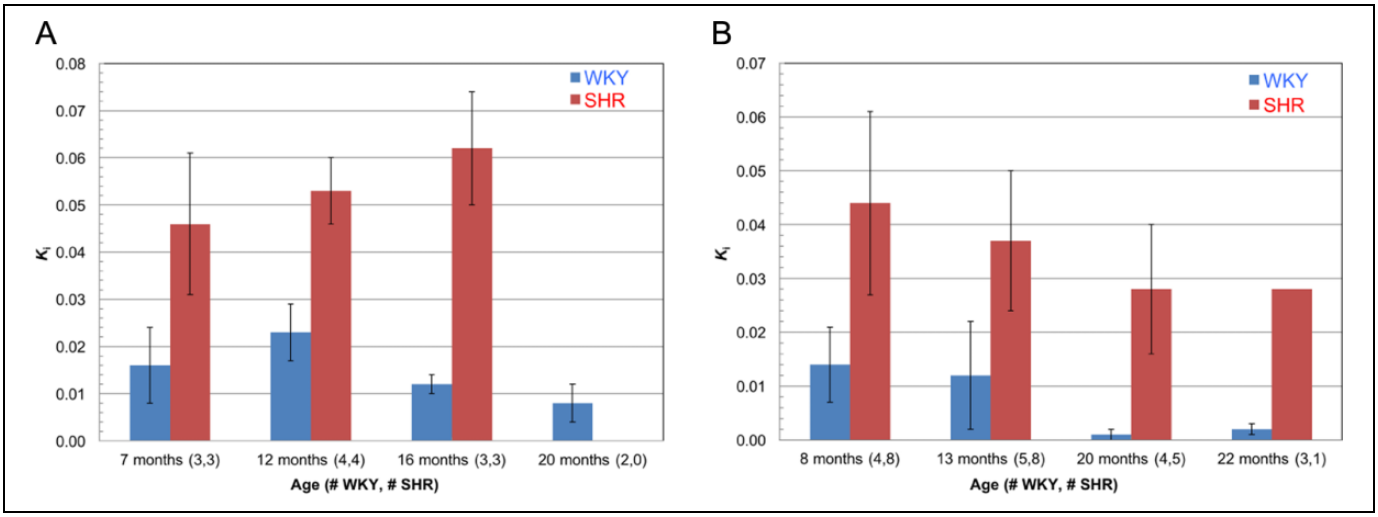

Figure 5. The ^{18}F-FDG influx rate constant K_i^{FDG} in myocardium as a function of age for the (A) 2009 to 2010 fed study and (B) 2011 to 2012 fasted study. The Patlak method[4,17] was used to calculate influx rate constant. FDG indicates fluorodeoxyglucose.

Table 2. Summary of Glucose Results.

	Fed	Fasted
FDG influx rate constant	SHR > WKY	SHR > WKY
Blood, glucose	SHR < WKY	SHR < WKY
Blood, insulin	SHR > WKY	Not significant

Abbreviations: FDG, fluorodeoxyglucose; SHR, spontaneously hypertensive rat; WKY, Wistar-Kyoto.

there was an age-dependent decrease seen in insulin concentrations when both models were pooled together ($P = .05$). In contrast, no significant dependency in insulin concentrations was observed with models pooled together when fed.

^{18}F-FTHA Kinetics in Myocardial Tissue (FA)

For both rat models and diet modalities, the TAC generated from each myocardial VOI displayed an increased ^{18}F-FTHA activity, followed by a plateau after roughly 4 minutes, and then a gradual decline that was faster than the blood (see Figure 2). The whole blood TAC showed a rapid washout from the blood.

The myocardial influx rate constant K_i^{FTHA} as a function of age for both animal models is shown in Figure 6. A 2-way ANOVA indicates that the SHRs demonstrated a significantly lower ^{18}F-FTHA myocardial influx rate constant K_i^{FTHA} than the WKY controls when fed ($P = .007$), whereas a reverse trend is seen when fasted but it was not significant ($P = .1$). An elevated rate of FA oxidation is expected at early time points due to fasting. As hypertrophy progressed in the SHR, we observed the expected downregulation of FA oxidation, but the trend was not significant within measurement errors.

A 2-way ANOVA of blood data indicates that FFA concentrations were significantly lower for the SHRs than the WKY controls under fed conditions ($P = 4 \times 10^{-4}$), whereas no significant difference was observed between models under fasting conditions ($P = .4$; Table 3). Although no significant difference was seen under fasting conditions, a significant interaction between rat model and time was manifested as an age-dependent increase for the SHR ($P < 7 \times 10^{-6}$).

Hypertrophy

Measurements of heart to body weight ratios of the SHRs were almost 2 times higher than the WKY rats at the time of death, which is indicative of a hypertrophied heart in the SHR model. For the 2009 to 2010 study, the heart to body weight ratio was 0.0037 $\pm$ 0.0006 at an average age of 20.4 $\pm$ 3.7 months for the WKY controls and 0.0062 $\pm$ 0.0013 at an average age of 18.3 $\pm$ 2.1 months for the SHRs. For the 2011 to 2012 study, all 8 SHRs developed hypertrophy with a life span of 20 $\pm$ 3 months. The heart to body weight ratio was 0.0037 $\pm$ 0.0003 for the controls and 0.0068 $\pm$ 0.0012 for the SHRs. Fluid in the lungs and dilated cavity volumes were also visible for the SHRs indicative of a hypertrophied heart with congestive HF.

Discussion

This is the first study to longitudinally monitor substrate shifts in myocardial FA and glucose metabolism, under both fed and fasted conditions, with in vivo imaging during the progression of HF in a rat model of LVH. This article presents the results of the 2009 to 2010 study when the rats were fed and compares these results with the 2011 to 2012 study[14] when the rats were fasted.

Metabolic Imaging

Our findings of increased glucose metabolism in the failing heart are consistent with findings in the literature.[20–22] Throughout all of our animal studies, glucose metabolism has

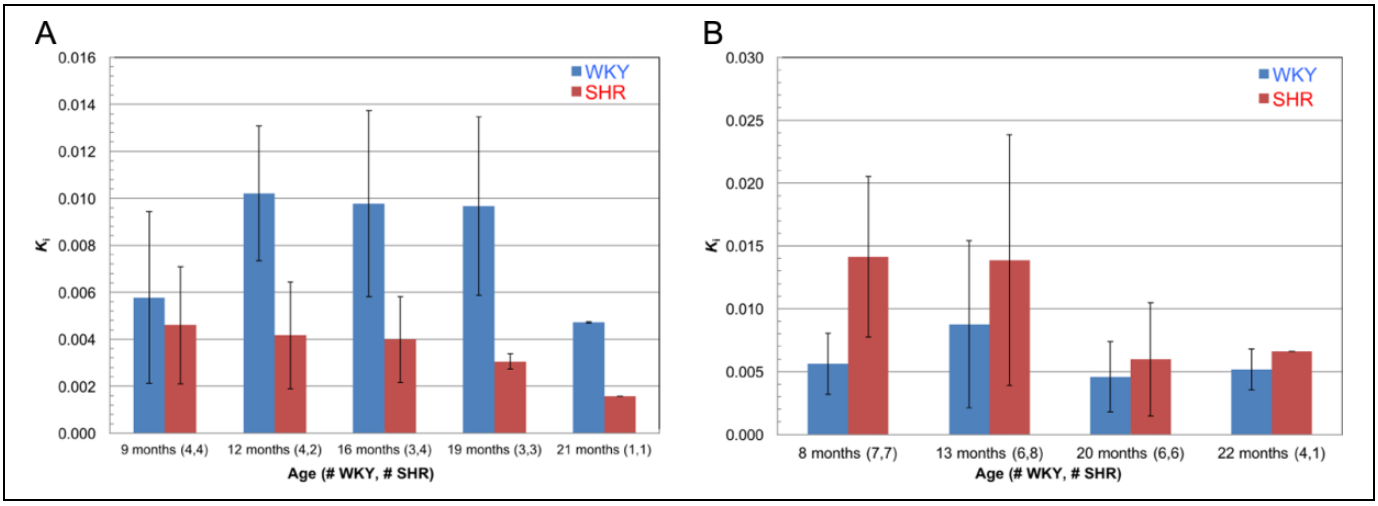

Figure 6. The ^{18}F-FTHA influx rate constant K_i^{FTHA} in myocardium as a function of age for the (A) 2009 to 2010 fed study and (B) 2011 to 2012 fasted study. The Patlak method[4,17] was used to calculate influx rate constant. FTHA indicates fluoro-6-thia-heptadecanoic acid.

Table 3. Summary of Fatty Acid Results.

	Fed	Fasted
FTHA influx rate constant	SHR < WKY	SHR > WKY
Blood, FFA	SHR < WKY	Not significant

Abbreviations: FFA, free fatty acids; FTHA, fluoro-6-thia-heptadecanoic acid; SHR, spontaneously hypertensive rat; WKY, Wistar-Kyoto.

been consistently greater in the hypertensive SHRs compared to WKY controls. In our preliminary 2003 to 2005 study,[23] even though this was a small sample size, glucose metabolism was observed to be greater in the SHR than the WKY control when fed and glucose metabolism decreased with age in both rat models. Whereas in our 2009 to 2010 study, there was no significant trend when fed for all animals ($P = .2$), though a decrease in glucose metabolism was observed with age in our 2011 to 2012 study when fasted ($P = .03$). Moreover, when fasted in our 2011 to 2012 study, a significant age-dependent increase in glucose plasma concentration was apparent in the controls ($P < 2 \times 10^{-5}$) but not in the SHRs. In addition, fasted insulin concentrations were significantly higher for the SHRs than the WKY rats ($P = 3 \times 10^{-3}$), whereas when fed, no significant difference was observed between models ($P = .4$). The higher insulin levels and lower glucose levels in the blood of the SHR model relative to control have been previously determined using the SHR model[13] and with HF patients.[3] The elevated insulin levels likely stimulate glucose uptake and metabolism by the heart. Additionally, we observed increased K_i^{FDG} in the SHR at early ages, 8 to 9 months, which is consistent with the findings of Hajri et al.[13]

The FA metabolism appeared lower for SHRs than WKYs with feeding, whereas a reverse trend was seen with fasting, but it was not significant. Our previous longitudinal study using dynamic single photon emission computed tomography (SPECT) imaging of ^{123}I- β-methyl-p-^{123}I-Iodophenyl-Pentadecanoic Acid (^{123}I-BMIPP) also indicated a higher FA metabolic rate when fed in 2 control rats compared with 2 SHRs at 14 months, as well as a general decrease in FA metabolic rate with age in both models.[19] Using the same FA analog BMIPP but tagged with ^{125}I, Hajri et al[13] found (different from us) reduced FA oxidation in the heart of the fasted SHRs compared with WKY controls. As age and LVH progressed in the SHRs in both the 2009 to 2010 study and the 2011 to 2012 study, we observed a hint of a downregulation of FA oxidation with age, but this trend was not significant with our measurement errors. We feel the differences in the FA uptake rate observed in our ^{123}I-BMIPP SPECT[24] and 2009 to 2010 ^{18}F-FTHA microPET studies and those of our 2011 to 2012 ^{18}F-FTHA microPET study are due to the fact that in the latter study the SHRs were fasted and in the former studies they were fed. For both rat models, fasting is expected to increase the circulating FFAs, which are preferentially oxidized by the heart. Although the measurement of circulating FFA plasma concentrations showed no significant difference between models when time was ignored ($P = .4$), an age-dependent increase in the SHR FFA levels relative to the control was seen ($P < 7 \times 10^{-6}$). A similar increase in plasma FFA concentrations has also been seen in HF patients in the late stages of the disease.[25] It has also been reported that a normal or slightly elevated rate of FA oxidation is observed at the early stage of HF, but as LVH progresses, there is a downregulation of FA oxidation.[3]

This longitudinal evaluation provided the ability to study metabolic changes during the progression of LVH in the SHR model. The PET/CT techniques used in this study could also be used to monitor substrate metabolism shifts in patients with LVH and potentially help improve diagnosis and therapy management. The separation of the trends with disease and age can be difficult because hypertrophy continues to increase with age as we observed in the measures of heart to body weight ratios. In advanced age of the normal rat, the resting myocardial oxygen consumption (MVO_2) and cardiac work remain intact; however, cardiac efficiency achieved at high demand are decreased with age, compared to the young.[26] It is possible that

during aging or pathological conditions, restricted diffusion of biochemical intermediates may lead to a decrease in the availability of the substrates.

Diabetes. It is well known that hypertension and diabetes frequently coexist and the combination causes more extensive structural and functional changes in the heart than either condition alone.[27–29] In our work, we did not study the effects of diabetes. Even though the SHR appears to be diabetic, we feel that the metabolic changes did not represent a diabetic condition. The SHR model has a genetic defect resulting in the deficiency of the membrane FA transporter CD36, which impairs transport of long-chain FAs across the cell membrane, causes hyperinsulinemia, and thus results in higher levels of insulin relative to glucose circulating in the blood. However, the SHR diabetic model is obtained with the added injection of streptozotocin. The streptozotocin causes the pancreas to swell and reduces β-cell mass (the insulin-producing cells) in the Langerhans islets of the pancreas.[30] Diabetes is made complete by glucotoxicity, causing secondary diabetic β-cell failure through hyperglycemia-stimulated pathways.[31] In one study, it was found that diabetes and hypertension impair the expression of α_1-adrenergic receptors (α_{1A} and α_{1D}) and angiotensin II receptors (AT_1 and AT_2) in the aorta after 4 weeks of the onset of diabetes.[32] In another study, it was found that apocynin reduces oxidative stress, commonly found with diabetes and hypertension, independently of nicotinamide adenine dinucleotide phosphate (NADPH) oxidase activity and does not change ventricular or myocardial function.[33] It has also been seen in the SHR diabetic model that enhancing the Ang-(1-7)-Mas-R-nNOS system was beneficial in preventing cardiovascular dysfunction and vulnerability related to diabetic hypertension.[34]

Imaging methods for early diagnosis of diabetes and for monitoring response to therapy fall into 2 categories: (1) directly imaging β-cells of the pancreas and (2) imaging brown adipose tissue (BAT) to follow therapy related to increasing energy expenditure of BAT for those with obesity and/or diabetes. While ^{18}F-FDG PET/CT is used in imaging pancreatic cancer, the most promising imaging tracers for imaging β-cell expression are those that target glucagon-like peptide 1 receptor (GLP-1R) as it is specifically expressed on β-cells, and exendin-4, a specific agonist of the receptor.[35] The PET/CT with ^{18}F-FDG is the most widely used method to image BAT.[36,37] Studies show that BAT activity is negatively correlated with body mass index and diabetic parameters and thus is a potential target for monitoring therapy for obesity and diabetes. The BAT demonstrates strong insulin and cold (without insulin) sensitivity with regard to glucose uptake, which suggests BAT performs functions of energy dissipation and thermoregulation. Imaging studies with ^{18}F-FDG in the SHR model also suggest that increased glucose utilization in BAT may be associated with higher sensitivity of adipose tissue to insulin action.[38]

Athletic heart. The athletic heart develops cardiac hypertrophy as a beneficial adaptation to exercise training.[39,40] The substrate utilization in the athletic heart is associated with enhanced FA and glucose oxidation, whereas pathological cardiac hypertrophy entails decreased FA oxidation and increased glycolysis.[39,41] This switch in substrate utilization in pathological cardiac hypertrophy contributes to the development of cardiac hypertrophy and failure.[42,43] The reduced FA oxidation in hypertrophied hearts in 16-week-old SHRs may be partly due to the downregulation of short-chain acyl-CoA dehydrogenase (SCAD), which is the enzyme in the conversion of butyryl-CoA to acetyl-CoA.[44] Compared with WKY rats, Huang et al[44] found that rates of glycolysis were significantly increased in the SHR, whereas rates of FA oxidation were significantly decreased with age in the SHR. Other studies with exercised training in Sprague-Dawley rats suggest that SCAD is significantly upregulated in exercise-induced cardiac hypertrophy.[45] Increasing the expression of SCAD by peroxisome proliferator-activated receptor alpha (PPAR-alpha) ligand fenofibrate treatment inhibited pathological cardiac hypertrophy.[44]

Perfusion Imaging

^{18}F-FDHROL demonstrated outstanding flow versus extraction characteristics, proving it to be an outstanding PET radiotracer for analyzing perfusion. In our experience compared with $^{18}NH_3$, ^{18}F-FDHROL provides improved contrast of the myocardium to background with very little uptake in the lung. Even though the SHR model was fed in both ^{18}F-FDHROL studies, it demonstrated a significantly higher wash-in rate constant ($P = 5 \times 10^{-6}$) and distribution volume ($P = 3 \times 10^{-8}$) than the WKY control for the 2011 to 2012 study, whereas no significant difference was observed for the 2009 to 2010 study ($P = 0.1$; Table 1). Previous results by others indicated that fasted SHRs showed an increase in perfusion compared to controls, corresponding to an increase in aerobic metabolism.[10] It may be that the increase in perfusion in our study was also an indication of an increased anaerobic metabolism because of the increase in glucose metabolism. It may also be due to increased aerobic metabolism, but we did not verify this—we did not fast the animals before the ^{18}F-FDHROL study and we did not measure perfusion at the exact same time as the glucose and FA metabolism during our 2011 to 2012 study.

Heart failure with preserved ejection fraction. The SHR model has also been used to study heart failure with preserved ejection fraction (HF-PEF), which leads to pulmonary congestion because of impaired diastolic filling. The HF-PEF affects those with a long history of hypertension or metabolic risk factors. Marzak et al[46] reported that aging SHRs develop HF-PEF as indicated by impaired LV relaxation, fibrosis, and hypertrophy, but contractility was preserved. As discussed above, in our studies, all SHRs developed hypertrophy as measured by the heart to body weight ratios. The SHRs also demonstrated a significant age-dependent increase in end-diastolic volume (EDV), whereas the control stayed constant with age.[14] This is in line with the results of Marzak et al[46] of impaired LV

relaxation. However, our results differ with that of Marzak et al[46] in that we saw early on a preserved left ventricular ejection fraction, but this significantly decreased in the second year of life, manifested as an age-dependent decrease in the SHR and an age-dependent increase in the control.[14] In the results by Marzak et al,[46] SHRs developed a progressive alteration of the early diastole, whereas systolic function evaluated by echocardiography and invasive catheterization was preserved. At the end of the longitudinal study, an increase in collagen synthesis and deposits was identified in subendocardial layers, which we have also observed.[47]

Limitations

The main limitations of these studies were the small sample size of animals and the limited physiological data without blood pressure and metabolite measurements. The 2009 to 2010 study began with 8 SHR and 8 WKY rats in the ^{18}F-FDHROL cohort; 4 SHR and 4 WKY rats in the ^{18}F-FDG cohort; and 4 SHR and 4 WKY rats in the ^{18}F-FTHA cohort. This study ended with 1 SHR and 4 WKY rats for the ^{18}F-FDHROL cohort; 0 SHR and 2 WKY rats for the ^{18}F-FDG cohort; and 1 SHR and 1 WKY rat for the ^{18}F-FTHA cohort during the last time point at approximately 18 months of age. The 2011 to 2012 study began with 8 SHR and 8 WKY rats and ended with 1 SHR and 4 WKY rats during the last time point at about 2 years of age. Thus, the value determined for any given parameter at the last time point is not very precise and is not representative of the entire cohort of SHRs. Experimental circumstances such as motion during the acquisition and inability to inject the tracer in the tail vein also limited the sample size at some time points.

^{18}F-FTHA is more complicated to model because of the slow release of metabolites from the myocardium. The ability to correct for these metabolites offers more accurate kinetic modeling. However, obtaining blood samples is a difficult task that can lead to serious blood depletion.

Conclusion

Longitudinal evaluation provides a means of studying metabolic changes during the progression of LVH in the SHR. In all of our imaging studies[14,23]—including the studies presented in this article—glucose metabolism is consistently elevated in the hypertensive SHRs compared to the normotensive WKY controls. The observed increase (though not significant) in FA metabolism with fasting in the SHR model was somewhat a surprise, because the reverse was observed in another study performed by others.[13] When fed the SHRs metabolized primarily glucose. As the 2009 to 2010 study and our previous work[19] showed, FA metabolism was less with the SHRs than with the WKY controls. The SHRs had an increase in perfusion for the 2009 to 2010 study, indicative of an increased aerobic metabolism, even though these animals were not fasted before the perfusion studies. The SHR animals also had greater distribution volumes than the WKY controls indicative of increased cardiac hypertrophy.

Hypertrophy was evidenced by the reliance on glucose oxidation-driven cardiac metabolism, elevated levels of circulating FFA and insulin plasma concentrations, lower levels of glucose plasma concentrations, and increased blood flow, which are needed to support the increased oxygen demands of the failing heart. In addition, hypertrophy was verified structurally by elevated EDV, increased heart to body weight ratios, and increased collagen content.

Our work and studies by others[48–51] clearly show that metabolism in LVH becomes maladaptive. Thus, there is a need for metabolic therapies that can improve cardiac performance and prevent or reverse the progression of LV dysfunction and remodeling.[3] The optimization of cardiac substrate metabolism using metabolic agents—such as FA oxidation inhibitors[3] or intervention with metformin[52] that improves glucose metabolism—may prevent a diminishing contractile function and a remodeling of cardiac structure in LVH. The techniques developed in our present imaging studies to monitor substrate metabolism shifts in the progression of LVH in rats could be translated to humans to help evaluate and develop therapeutic protocols directed at preventing and managing LVH. The use of animal models is valuable in studying the many facets of the disease process.

Acknowledgments

The authors thank Rod Gullberg of Clearview Statistical Consulting for his assistance with the statistical analyses.

Declaration of Conflicting Interests

The author(s) declared no potential conflicts of interest with respect to the research, authorship, and/or publication of this article.

Funding

The author(s) disclosed receipt of the following financial support for the research, authorship, and/or publication of this article: This study was supported by the National Institutes of Health of the US Department of Health and Human Services under grant R01-EB007219 and by the Director, Office of Science, Office of Biological and Environmental Research of the US Department of Energy under contract DE-AC02-05CH11231.

References

1. Neely JR, Morgan HE. Relationship between carbohydrate and lipid metabolism and the energy balance of heart muscle. *Annu Rev Physiol*. 1974;36:413–459.
2. Bing RJ, Siegel A, Ungar I, Gilbert M. Metabolism of the human heart. II. Studies on fat, ketone and amino acid metabolism. *Am J Med*. 1954;16(4):504–515.
3. Stanley WC, Recchia FA, Lopaschuk GD. Myocardial substrate metabolism in the normal and failing heart. *Physiol Rev*. 2005; 85(3):1093–1129.
4. Taylor M, Wallhaus TR, Degrado TR, et al. An evaluation of myocardial fatty acid and glucose uptake using PET with [^{18}F]fluoro-6-thia-heptadecanoic acid and [^{18}F]FDG in patients with congestive heart failure. *J Nucl Med*. 2001;42(1):55–62.

5. de las Fuentes L, Herrero P, Peterson LR, Kelly DP, Gropler RJ, Dávila-Román VG. Myocardial fatty acid metabolism: independent predictor of left ventricular mass in hypertensive heart disease. *Hypertension*. 2003;41(1):83–87.
6. DeGrado TR, Coenen HH, Stocklin G. 14(R,S)-[^{18}F]fluoro-6-thia-heptadecanoic acid (FTHA): evaluation in mouse of a new probe of myocardial utilization of long chain fatty acids. *J Nucl Med*. 1991;32(10):1888–1896.
7. Maki MT, Haaparanta M, Nuutila P, et al. Free fatty acid uptake in the myocardium and skeletal muscle using fluorine-18-fluoro-6-thia-heptadecanoic acid. *J Nucl Med*. 1998;39(8):1320–1327.
8. Katz AM. Mechanisms and abnormalities of contractility and relaxation in the failing heart. *Cardiologia*. 1993;38(12 suppl 1):39–43.
9. Granstam SO, Granstam E, Fellström B, Lind L. Regional haemodynamic differences between normotensive and spontaneously hypertensive rats—a microsphere study. *Physiol Res*. 1998;47(1): 9–15.
10. Nishiyama K, Nishiyama A, Frohlich ED. Regional blood flow in normotensive and spontaneously hypertensive rats. *Am J Physiol*. 1976;230(3):691–698.
11. Bing OH, Brooks WW, Robinson KG, et al. The spontaneously hypertensive rat as a model of the transition from compensated left ventricular hypertrophy to failure. *J Mol Cell Cardiol*. 1995; 27(1):383–396.
12. Brooks WW, Shen SS, Conrad CH, Goldstein RH, Bing OH. Transition from compensated hypertrophy to systolic heart failure in the spontaneously hypertensive rat: structure, function, and transcript analysis. *Genomics*. 2010;95(2):84–92.
13. Hajri T, Ibrahimi A, Coburn CT, et al. Defective fatty acid uptake in the spontaneously hypertensive rat is a primary determinant of altered glucose metabolism, hyperinsulinemia, and myocardial hypertrophy. *J Biol Chem*. 2001;276(26):23661–23666.
14. Hernandez AM, Murphy ST, Zeng GL, et al. Longitudinal evaluation of left ventricular substrate metabolism, perfusion, and dysfunction in the SHR model of hypertrophy using microPET imaging. *J Nucl Med*. 2013;54(11):1938–1945.
15. Janabi M, Gullberg GT, O'Neil JP. The use of GE's automated synthesis module (FxFN) for the production of [^{18}F]fluorodihydrorotenol (FDHROL) and [^{18}F]fluoro-thia-6-heptadecanoic acid [abstract]. *J Label Compd Radiopharm*. 2011;54(S1): S431.
16. Zeng GL, Hernandez A, Kadrmas DJ, Gullberg GT. Kinetic parameter estimation using a closed-form expression via integration by parts. *Phys Med Biol*. 2012;57(18):5809–5821.
17. Patlak CS, Blasberg RG, Fenstermacher JD. Graphical evaluation of blood-to-brain transfer constants from multiple-time uptake data. *J Cereb Blood Flow Metab*. 1983;3(1):1–7.
18. Logan J. Graphical analysis of PET data applied to reversible and irreversible tracers. *Nucl Med Biol*. 2000;27(7):661–670.
19. Fueger BJ, Czernin J, Hildebrandt I, et al. Impact of animal handling on the results of ^{18}F-FDG PET studies in mice. *J Nucl Med*. 2006;47(6):999–1006.
20. Taylor M, Wallhaus TR, Degrado TR, et al. An evaluation of myocardial fatty acid and glucose uptake using PET with [^{18}F]fluoro-6-thia-heptadecanoic acid and [^{18}F]FDG in patients with congestive heart failure. *J Nucl Med*. 2001;42(1):55–62.
21. Dávila-Román VG, Vedala G, Herrero P, et al. Altered myocardial fatty acid and glucose metabolism in idiopathic dilated cardiomyopathy. *J Am Coll Cardiol*. 2002;40(2):271–277.
22. Dodd MS, Ball DR, Schroeder MA, et al. In vivo alterations in cardiac metabolism and function in the spontaneously hypertensive rat heart. *Cardiovasc Res*. 2012;95(1):69–76.
23. Gullberg GT, Huesman RH, Reutter BW, et al. A study of changes in deformation and metabolism in the left ventricle as a function of hypertrophy in SHR rats using microPET technology: *International Conference of Nuclear Cardiology, Lisbon, Portugal*, *May* 8-11, 2005. Lawrence Berkeley National Lab Report LBNL-1006557; 2016, Berkeley, CA: Lawrence Berkeley National Laboratory, University of California.
24. Reutter BW, Huesman RH, Brennan KM, Boutchko R, Hanrahan SM, Gullberg GT. Longitudinal evaluation of fatty acid metabolism in normal and spontaneously hypertensive rat hearts with dynamic MicroSPECT imaging. *Int J Mol Imaging*. 2011;2011: 893129.
25. Paolisso G, Gambardella A, Galzerano D, et al. Total-body and myocardial substrate oxidation in congestive heart failure. *Metabolism*. 1994;43(2):174–179.
26. Yaniv Y, Juhaszova M, Sollott SJ. Age-related changes of myocardial ATP supply and demand mechanisms. *Trends Endocrinol Metab*. 2013;24(10):495–505.
27. Falcão-Pires I, Palladini G, Gonçalves N, et al. Distinct mechanisms for diastolic dysfunction in diabetes mellitus and chronic pressure-overload. *Basic Res Cardiol*. 2011;106(5):801–814.
28. Rosa CM, Xavier NP, Henrique Campos D, et al. Diabetes mellitus activates fetal gene program and intensifies cardiac remodeling and oxidative stress in aged spontaneously hypertensive rats. *Cardiovasc Diabetol*. 2013;12:152.
29. Gonçalves N, Gomes-Ferreira C, Moura C, Roncon-Albuquerque R Jr, Leite-Moreira AF, Falcão-Pires I. Worse cardiac remodeling in response to pressure overload in type 2 diabetes mellitus. *Int J Cardiol*. 2016;217:195–204.
30. Akbarzadeh A, Norouzian D, Mehrabi MR, et al. Induction of diabetes by Streptozotocin in rats. *Indian J Clin Biochem*. 2007; 22(2):60–64.
31. Liang W, Yan LJ. Streptozotocin-induced type 1 diabetes in rodents as a model for studying mitochondrial mechanisms of diabetic β cell glucotoxicity. *Diabetes Metab Syndr Obes*. 2015;8:181–188.
32. Rodríguez JE, Romero-Nava R, Reséndiz-Albor AA, et al. Expression and localization of the AT1 and AT2 angiotensin II receptors and α1A and α1D adrenergic receptors in aorta of hypertensive and diabetic rats. *Clin Exp Hypertens*. 2017;39(1): 85–92.
33. Rosa CM, Gimenes R, Campos DH, et al. Apocynin influence on oxidative stress and cardiac remodeling of spontaneously hypertensive rats with diabetes mellitus. *Cardiovasc Diabetol*. 2016; 15(1):126.
34. Li H, Liu X, Ren Z, et al. Effects of diabetic hyperglycemia on central Ang-(1-7)-Mas-R-nNOS pathways in spontaneously hypertensive rats. *Cell Physiol Biochem*. 2016;40(5):1186–1197.
35. Jodal A, Schibli R, Béhé M. Targets and probes for non-invasive imaging of β-cells. *Eur J Nucl Med Mol Imag*. 2017;44(4): 712–727.

36. Izzi-Engbeaya C, Salem V, Atkar RS, Dhillo WS. Insights into brown adipose tissue physiology as revealed by imaging studies. *Adipocyte*. 2015;4(1):1–12.
37. Sampath SC, Sampath SC, Bredella MA, Cypess AM, Torriani M. Imaging of brown adipose tissue: state of the art. *Radiology*. 2016; 280(1):4–19.
38. Trnovská J, Šilhavý J, Zídek V, et al. Gender-related effects on substrate utilization and metabolic adaptation in hairless spontaneously hypertensive rat. *Physiol Res*. 2015;64(1):51–60.
39. Iemitsu M, Miyauchi T, Maeda S, et al. Cardiac hypertrophy by hypertension and exercise training exhibits different gene expression of enzymes in energy metabolism. *Hypertens Res*. 2003; 26(10):829–837.
40. Bernardo BC, Weeks KL, Pretorius L, McMullen JR. Molecular distinction between physiological and pathological cardiac hypertrophy: experimental findings and therapeutic strategies. *Pharmacol Ther*. 2010;128(1):191–227.
41. Abel ED, Doenst T. Mitochondrial adaptations to physiological vs. pathological cardiac hypertrophy. *Cardiovasc Res*. 2011; 90(2):234–242.
42. Dodd MS, Ball DR, Schroeder MA, et al. In vivo alterations in cardiac metabolism and function in the spontaneously hypertensive rat heart. *Cardiovasc Res*. 2012;95(1):69–76.
43. Rosca MG, Tandler B, Hoppel CL. Mitochondria in cardiac hypertrophy and heart failure. *J Mol Cell Cardiol*. 2013;55:31–41.
44. Huang J, Xu L, Huang Q, et al. Changes in short-chain acyl-coA dehydrogenase during rat cardiac development and stress. *J Cell Mol Med*. 2015;19(7):1672–1688.
45. Sun B, Wang JH, Lv YY, Zhu SS, Yang J, Ma JZ. Proteomic adaptation to chronic high intensity swimming training in the rat heart. *Comp Biochem Physiol Part D Genomics Proteomics*. 2008;3(1):108–117.
46. Marzak H, Ayme-Dietrich E, Lawson R, et al. Old spontaneously hypertensive rats gather together typical features of human chronic left-ventricular dysfunction with preserved ejection fraction. *J Hypertens*. 2014;32(6):1307–1016.
47. Giannakidis A, Rohmer D, Veress AI, Gullberg GT. Chapter 53: diffusion tensor MRI-derived myocardial fiber disarray in hypertensive left ventricular hypertrophy: visualization, quantification and the effect on mechanical function. In: Shenasa M, Hindricks G, Borggrefe M, Breithardt G, Josephson ME, eds. *Cardiac Mapping*. Chichester, UK: Blackwell Publishing Limited; 2013.
48. Davila-Roman VG, Vedala G, Herrero P, et al. Altered myocardial fatty acid and glucose metabolism in idiopathic dilated cardiomyopathy. *J Am Coll Cardiol*. 2002;40(2): 271–277.
49. Dodd MS, Ball DR, Schroeder MA, et al. In vivo alterations in cardiac metabolism and function in the spontaneously hypertensive rat heart. *Cardiovasc Res*. 2012;95(1):69–76.
50. de las Fuentes L, Soto PF, Cupps BP, et al. Hypertensive left ventricular hypertrophy is associated with abnormal myocardial fatty acid metabolism and myocardial efficiency. *J Nucl Cardiol*. 2006;13(3):369–377.
51. Taegtmeyer H, Wilson CR, Razeghi P, Sharma S. Metabolic energetics and genetics in the heart. *Ann N Y Acad Sci*. 2005; 1047:208–218.
52. Kundu BK, Zhong M, Sen S, Davogustto G, Keller SR, Taegtmeyer H. Remodeling of glucose metabolism precedes pressure overload-induced left ventricular hypertrophy: review of a hypothesis. *Cardiology*. 2015;130(4):211–220.